Chapter 4

Holocene monsoon variability

The Holocene (Greek meaning = entirely new) period beginning at 11,700 yr BP, is the most recent interglacial period and is also known as the Marine Isotope stage -1(MIS-1). Climatic fluctuations within the Holocene were presumed to be less significant compared to the major glacial-interglacial variations. However, Holocene paleoclimate reconstructions have gained more importance with the discovery of oscillations with a pacing similar to the climatic events during the glacial periods (∼1500 year cycle) [*Bond et al.*, 1997, 2001; *Bond and Lotti*, 1995; *Broecker and Hemming*, 2001; *O'brien et al.*, 1995]. These cycles are considered to be Holocene extensions of Dansgaard-Oeschger oscillaitons which are recorders of THE North-Atlantic climate changes during the last glacial period. Since these oscillations occurred in similar climatic conditions as today (warmer, and absence of large Hemispheric ice sheets), they are directly related to the understanding of the contemporary climate change rather than the glacial climate change. The discussions about the cyclic nature of these changes gained momentum after observing transitions from the Medieval warm period (MWP) to Little Ice Age(LIA), which is the most recent advance of glaciers in the Holocene [*Wanner et al.*, 2008]. These abrupt climatic changes also have had a large impact on rise and fall of human civilizations [*Enzel et al.*, 1999]. In response to interglacial warming, the Indian monsoon steadily increased at the beginning

of Holocene, as shown by several comprehensive studies [*Mayewski et al.*, 2004; *Tiwari et al.*, 2011]. However, some consensus still exists that the Holocene experienced a countrywide aridification [*Ponton et al.*, 2012]. To test both these hypotheses it's important to generate high resolution records of ISM from the core monsoon region of India. The focus of this chapter is on climate variability during the Holocene and establish the link between global climate events and the Indian summer monsoon.

4.1 The Dandak-I stalagmite

The stalagmite sample was collected in February 1996, 220 m inside the cave.The temperature and humidity of the cave atmosphere were 27℃ and 92%, respectively. To determine the moisture sources contributing to rainfall during the wet season (June to October), we carried out a Lagrangian back trajectory analysis using the HYSPLIT model [*Stein et al.*, 2015] with NCEP Reanalysis-1 [*Kalnay et al.*, 1996] as input to the model. We chose all the days with daily rain above 2 mm during 5 years (1980 to 2009 CE) for the analysis. During ISM, trajectories suggest that the Arabian Sea is the major source of moisture and its isotopic composition is likely to reflect the rainout over the Western Ghat region Figure (4.1).

4.1.1 Mineralogy

The mineralogical composition of the stalagmite was studied based on thin sections prepared at the M.S.University of Baroda,Vadodara. The sections were analyzed under a camera aided petrological microscope Leica DM EP. A section was also prepared across the hiatus boundary to check for the textural changes prior to the subsequent deposition. The stalagmite sample is composed of calcite. Figure 4.2 (a) and (b) show one such section where the layers are made up of columnar calcite fabric. Thin laminations are seen as altered dark layers. The

hiatus as shown in Figure 4.2 is an erosional boundary, with the growth of calcite crystals occurred on both the sides.
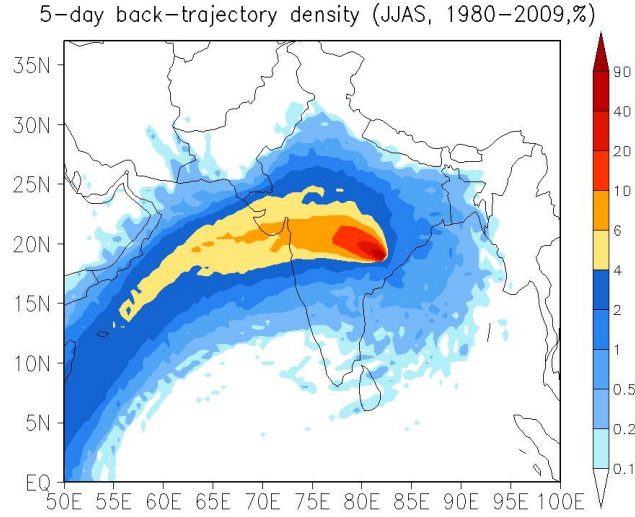

Figure 4.1: *Climatological monthly rainfall in a 0.5 × 0.5 grid over the Dandak cave. Climatology is calculated using Asian Precipitation-Highly-Resolved Observational Data Integration Towards Evaluation (APHRODITE) data from CE 1980-2009 [Yatagai et al., 2012].*
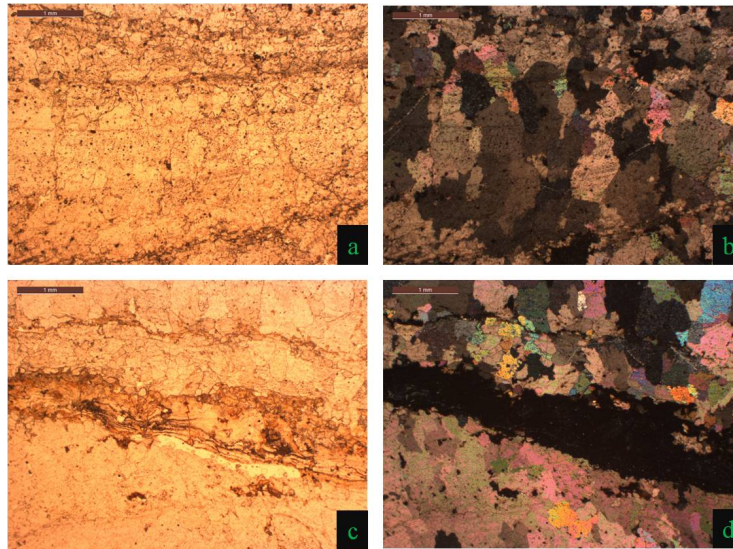

Figure 4.2: *a) and b) are plane polarized light (ppl) and cross polarized light (xpl) images of DAN-I stalagmite, respectively. The entire sample is composed of columnar calcite fabric. c) and d) are ppl and xpl images of the sample across the hiatus. The hiatus is seen as a dark opaque band, with no deposition. Euhedral crystals of calcite are seen on both sides of the hiatus.*

4.1.2   U-Th ages

Fourteen U-Th ages were obtained from the $\sim$ 29 cm long Dan-I stalagmite. The sample was dated in the University of New Mexico, and the U-Th ages are shown in Table 4.1. Corrected ages use an initial $^{230}Th/^{232}Th$ atomic ratio $= 0.0012 \times^{232} Th^{-0.6386}$ where, ^{232}Th is concentration in parts per million (ppt), with the supposition that lower concentration of ^{232}Th equates with higher $^{230}Th/^{232}Th$ ratios. Years before present $=$ yr BP, where present is AD 2007. Subsamples weighing $\sim 90 - 408$ mg were used. The ages have five distinct tractable reversals, superimposing at 1σ error limit. An interactive tool, COPRA, was used to generate an age model shown in Figure 4.3. Since the sample was active (dripping on the stalagmite) during its collection, age zero was introduced in the model at the tip of the sample. The sample shows a brief hiatus at the depth of 21.7 cm, post which, the growth layers are continuous. Based on the age model, the stalagmite growth began at $\sim$ 6.5 ka BP, with a cessation at $\sim$ 2.2 ka BP. After the hiatus of 200 years, the sample growth resumed at $\sim$ 2.0 ka BP to the present.
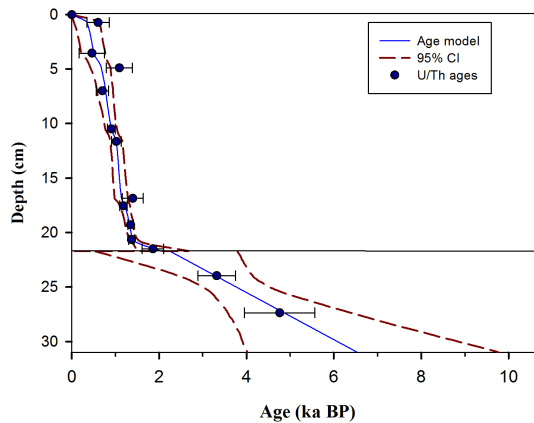

Figure 4.3: *Age model reconstructed using COPRA- an interactive program on MATLAB [Breitenbach et al., 2012]. The filled blue circles are ^{230}Th ages used in the age model. The errors are reported as 2σ. The dashed lines show 95% confidence intervals and the blue line is the median through which the age model passes.*

Table 4.1: *Uranium and Thorium isotopic compositions and ^{230}Th ages of the subsamples of Dandak-I stalagmite.All the errors are reported in 2σ.*

Sample	^{238}U (ppb)	^{232}Th (ppt)	$^{230}Th/^{232}Th$ activity ratio	$^{230}Th/^{238}U$ activity ratio	measured $\delta^{234}U$ (‰)	initial $\delta^{234}U$ (‰)	uncorrected age Yr BP	corrected age Yr BP
1M(7.4 mm)	313.3±0.8	11409 ± 52	1.2 ± 0.0	0.0148 ± 0.0004	461 ± 2	461 ± 2	1688 ± 61	602 ± 509
top1(34.4 mm)	227.2 ± 1	10486 ± 55	0.9 ± 0.2	0.0131 ± 0.0036	442 ± 11	442 ± 12	993 ± 278	304 ± 743
top1-2(34.4 mm)	226.8±0.8	10884 ± 69	1.2 ± 0.5	0.0185 ± 0.0079	454 ± 5	454 ± 5	1400 ± 602	705 ± 918
40M (40.5 mm)	141.4±0.3	1931 ± 39	5.0 ± 0.2	0.0223 ± 0.0008	451 ± 2	452 ± 2	1688 ± 61	1091 ± 600
63M (65.3 mm)	193.5±0.5	574 ± 32	13.4 ± 0.9	0.0130 ± 0.0005	447 ± 1	448 ± 1	984 ± 35	702 ± 284
93M (95.9 mm)	217.9±0.6	230 ± 41	41.4 ± 7.6	0.0143 ± 0.0005	444 ± 2	445 ± 2	1087 ± 39	907 ± 187
P (106.9 mm)	359.4±2.6	3763 ± 22	4.9 ± 0.2	0.0169 ± 0.0007	444 ± 8	445 ± 8	1285 ± 51	985 ± 304
P2 (106.9 mm)	358.8±2.6	3944 ± 30	5.0 ± 0.5	0.0180 ± 0.0017	439 ± 9	440 ± 9	1373 ± 128	1067 ± 220
126M (129.3 mm)	330.8±0.8	331 ± 1	44.1 ± 4.9	0.0208 ± 0.0005	442 ± 1	444 ± 1	1583 ± 38	1428 ± 160
155M (159.9 mm)	423.1±1.1	22089 ± 68	1.4 ± 0.0	0.0247 ± 0.0004	445 ± 1	447 ± 2	1879 ± 30	1397 ± 484
N (164.6 mm)	325.0±1.5	939 ± 12	20.3 ± 1	0.0192 ± 0.0010	445 ± 6	447 ± 6	1460 ± 73	1260 ± 213
N2 (164.6 mm)	325.2±2.2	973 ± 12	18.5 ± 0.9	0.0181 ± 0.0008	438 ± 11	439 ± 11	1381 ± 64	1177 ± 214
174M (180.4 mm)	415.6 ± 1	535 ± 42	46.0 ± 3.7	0.0194 ± 0.0003	442 ± 1	443 ± 1	1477 ± 26	1348 ± 131
200M (204.1 mm)	316.7±0.8	2821 ± 43	7.5 ± 0.2	0.0219 ± 0.0005	439 ± 2	441 ± 2	1675 ± 36	1368 ± 310
G (210.0 mm)	361.6±2.6	32564±131	1.1 ± 0.1	0.0312 ± 0.0020	442 ± 11	444 ± 11	2389 ± 158	1737 ± 670
G2(210.0 mm)	360.2±2.6	32873±132	1.2 ± 0.1	0.0347 ± 0.0038	443 ± 17	446 ± 17	2653 ± 298	1998 ± 719
213M (221.2 mm)	284.5±0.7	35045 ± 90	1.3 ± 0.0	0.0538 ± 0.0007	0 ± 0	436 ± 2	4175 ± 58	3319 ± 858
D (253 mm)	136.3±0.6	24204 ± 70	1.4 ± 0.1	0.0808 ± 0.0053	433 ± 11	439 ± 12	6323 ± 430	4759±1621

Corrected ages use an initial $^{230}Th/^{232}Th$ atomic ratio $= 0.0012 \times^{232} Th^{-0.6386}$, where ^{232}Th is concentration in ppt, with the supposition that lower concentration of ^{232}Th equates with higher $^{230}Th/^{232}Th$ ratios. Years before present = yr BP, where present is AD 2007. Subsample sizes range from 90 to 408 mg. Distances from the tops of the stalagmites are incorporated into the subsample names.

4.1.3 Stable isotopes of oxygen and carbon

The $\delta^{18}O$ time series of the Dandak-I stalagmite is shown in Figure 4.4. The $\delta^{18}O$ (blue) values range from -6 to -2‰, whereas the $\delta^{13}C$ (purple) values vary between -11 to -3‰. The ages with 2σ errors are shown in orange filled circles. The $\delta^{18}O$ values show a slow decrease from 6.5 ka BP to present, with episodes of enrichment between 6-5 ka,4.7-4.2 ka and 0.8-0.4 ka BP. The $\delta^{13}C$ data follow a similar trend, however the peak observed at 3.5-2.5 ka BP in $\delta^{18}O$ values is not seen. There is sharp enrichment in the values for the span of hundred years

Table 4.2: *Uranium and Thorium isotopic compositions and ^{230}Th ages of the subsamples of Dandak- II stalagmite.All errors are absolute 2σ values.*

Sample	^{238}U (ppb)	^{232}Th (ppt)	$^{230}Th/^{232}Th$ activity ratio	$^{230}Th/^{238}U$ activity ratio	measured $\delta^{234}U$ (‰)	initial $\delta^{234}U$ (‰)	uncorrected age Yr BP	corrected age Yr BP
top2(13.5mm)	266.7±1.7	2442 ± 25	46.9 ± 1.1	0.1406 ± 0.0030	695 ± 11	713 ± 11	9398 ± 217	9107 ± 363
top2-2(13.5 mm)	266.4±1.3	2412 ± 80	49.1 ± 2.2	0.1454 ± 0.0042	700 ± 13	709 ± 13	9706 ± 305	9417 ± 420
top1-2(avg)							weight average age =	9420 ± 270
stest (61.0 mm)	222.8±1.1	5040 ± 44	19.8 ± 0.6	0.1464 ± 0.0045	692 ± 11	711 ± 11	9825 ± 324	9371 ± 557
K (189 mm)	178.9±0.8	187 ± 18	437.1 ± 43.2	0.1492 ± 0.0030	683 ± 10	702 ± 10	10080 ± 221	9907 ± 280
K2 (189 mm)	179.3±0.8	203 ± 18	400.0 ± 39	0.1485 ± 0.0053	697 ± 9	717 ± 9	9983 ± 371	9762 ± 411
K(avg)							weight average age =	9861 ± 230
B(319.5 mm)	322.9±1.7	1343 ± 18	114.7 ± 3.4	0.1560 ± 0.0041	693 ± 9	713 ± 10	10492 ± 296	10298±353
B2 (319.5 mm)	323.6±1.4	1386 ± 16	109.2 ± 2.0	0.1529 ± 0.002	695 ± 8	715 ± 8	10262 ± 163	10067±254
B(avg)							weight average age =	10146±210

Corrected ages use an initial $^{230}Th/^{232}Th$ atomic ratio $= 0.0012 \times^{232} Th^{-0.6386}$, where ^{232}Th is concentration in ppt, with the supposition that lower concentration of ^{232}Th equate to higher $^{230}Th/^{232}Th$ ratios. Years before present = yr BP, where present is AD 2007. Subsample sizes range from 90 to 408 mg. Distances from the tops of the stalagmites are incorporated into the subsample names.

between 0.6 - 0.7 ka BP.

4.1.4 Trace element analysis

The interpretation of trace element data of the Dan-I stalagmite were already discussed in *Yadava* [2002]; *Yadava and Ramesh* [2001](Figure 4.5). The trace element values in this study are useful as a supporting evidence to the $\delta^{18}O$ values, in paleomonsoon reconstruction. The variations in the trace element concentrations of Mg,Sr and Ba, were measured on ICP-AES (Inductively Coupled Plasma Atomic Emission Spectroscopy). The concentrations of the elements are reported in parts per million (ppm). Since the measurements of Ca ions were not carried out, normalization of trace elements with respect to calcium was not possible. Nevertheless, bare concentrations can be taken as indicators of PCP or high influx of meteoric water. The age model for trace elements was generated using

Table 4.3: *Uranium and Thorium isotopic compositions and ^{230}Th ages of the subsamples of Kotumsar stalagmite. All errors are absolute 2σ values.*

Sample	^{238}U (ppb)	^{232}Th (ppt)	$^{230}Th/^{232}Th$ activity ratio	$^{230}Th/^{238}U$ activity ratio	measured $\delta^{234}U$ (‰)	initial $\delta^{234}U$ (‰)	uncorrected age Yr BP	corrected age Yr BP
KOT-1 (1.5 mm)	244.34± 0.2	79.5 ± 4.5	0.08192 ± 0.000067	4152 ± 237	622.8±1.4	632.8±1.4	5631 ± 48	5626 ± 48
KOT-2 (11.5 mm)	80.531± 0.064	1281.3 ± 5	0.1386 ± 0.0012	143.6 ± 1.3	688.1±1.5	705.9±1.6	9287 ± 82	9040±148
KOT-3 (23 mm)	78.246± 0.062	282.1 ± 4.1	0.2034 ± 0.0012	930 ± 15	693.1±1.7	720.6±1.7	13841 ± 90	13.785 ± 94
KOT-4 (38 mm)	73.557± 0.059	3142 ± 7.6	0.1362 ± 0.0017	52.5 ± 0.067	684.9±1.8	701.5±1.9	9142 ± 120	8476±355
KOT-5 (46 mm)	84.213± 0.068	1402 ± 4.1	0.1325 ± 0.0010	132.2 ± 1.1	686.2±1.7	703.3±1.7	8948 ± 72	8690±148
KOT-6 (62.5 mm)	74.826± 0.074	230.2 ± 4	0.1517 ± 0.0011	813 ± 15	696.5±2.7	716.7±2.8	10153 ± 81	10105±84
KOT-7 (78.5 mm)	77.818± 0.070	315.1 ± 2.7	0.10064 ± 0.00078	409.7 ± 4.7	696 ± 2.1	709.1±2.2	6644 ± 53	6581 ± 62
KOT-8 (103 mm)	95.443± 0.092	173.8 ± 1.7	0.10148 ± 0.00057	919 ± 11	696.9±2.7	710.1±2.8	6697 ± 40	6669 ± 43
KOT-9 (124 mm)	86.547± 0.079	629.8 ± 2.1	0.09881 ± 0.00065	223.9 ± 1.6	700.4±2.2	713.2±2.3	6503 ± 45	6391 ± 72
KOT-10 (168 mm)	101.609± 0.0.095	2063 ± 34	0.1012 ± 0.0012	82.2 ± 1.6	715.7±2.3	728.6±2.3	6603 ± 78	6292±174
KOT-11 (181.5mm)	117.40± 0.13	2057.4 ± 4.3	0.1031 ± 0.0010	97 ± 1	706.7±2.5	719.8±2.6	6767 ± 68	6497±151
KOT-12 (201 mm)	321.88± 0.064	4581 ± 73	0.648 ± 0.0019	751 ± 25	409.3±3.7	491.2±5.7	64857 ± 2545	64604 ± 2542
KOT-13 (227 mm)	114.50± 0.12	16518 ± 70	0.3967 ± 0.0064	45.3 ± 0.76	719.7±2.8	774.2±4	28072 ± 510	25903 ± 1206
KOT-14 (274 mm)	120.68± 0.11	7561 ± 20	0.1298 ± 0.0022	34.1 ± 0.59	674.6±2.1	689.6±2.3	8755 ± 156	7770±519
KOT-15 (276.5mm)	93.198± 0.084	763 ± 4	0.1195 ± 0.0010	240.9 ± 2.5	684.8±2.0	700.1±2.0	7+87±72	7860 ± 96

The degree of detrital ^{230}Th contamination is indicated by the $^{230}Th/^{232}Th$ atomic ratio instead of the activity ratio. Age corrections for samples were calculated using an estimated initial atomic $^{230}Th/^{232}Th$ ratio of 4 ± 4 ppm. Decay constants are $9.1705 \times 10^{-6} yr^{-1}$ for ^{230}Th, $2.8221 \times 10^{-6} yr^{-1}$ for ^{234}U [Cheng et al., 2013], and $1.55125 \times 10^{-10} yr^{-1}$ for ^{238}U [Mattinson, 2000].
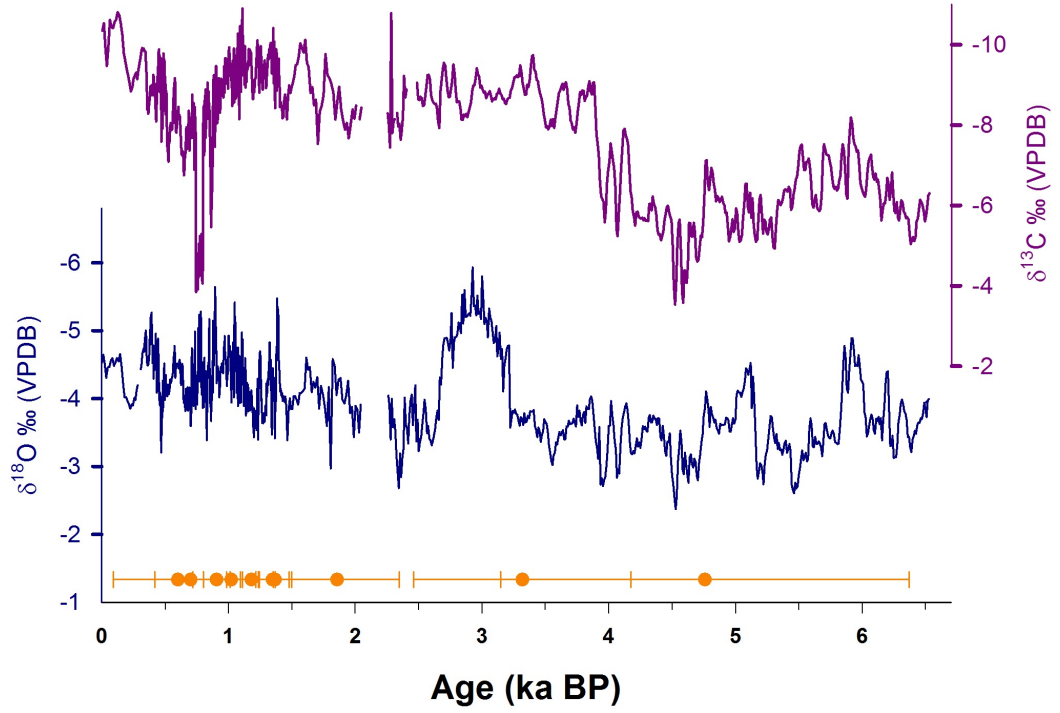
Figure 4.4: $\delta^{18}O$ *(Dark blue) and* $\delta^{13}C$ *(Purple) profiles of the Dandak-I stalagmite. The timeseries represents the profile based on ages derived from the COPRA age model. The ages considered in the model are shown as orange filled circles. The errors are reported as* 2σ.

COPRA and the timeseries is shown in Figure 4.5. Since the trace element and $\delta^{18}O$ measurements were carried out on different stalagmite slices, there is a shift in the time-series, owing to different sampling depths (indicated by the arrows). From $\sim$ 2 ka to the present the trace element concentrations and $\delta^{18}O$ values covary. The concentrations drop abruptly between 3.5 - 2.8 ka BP, showing peak to peak matching with $\delta^{18}O$ values.
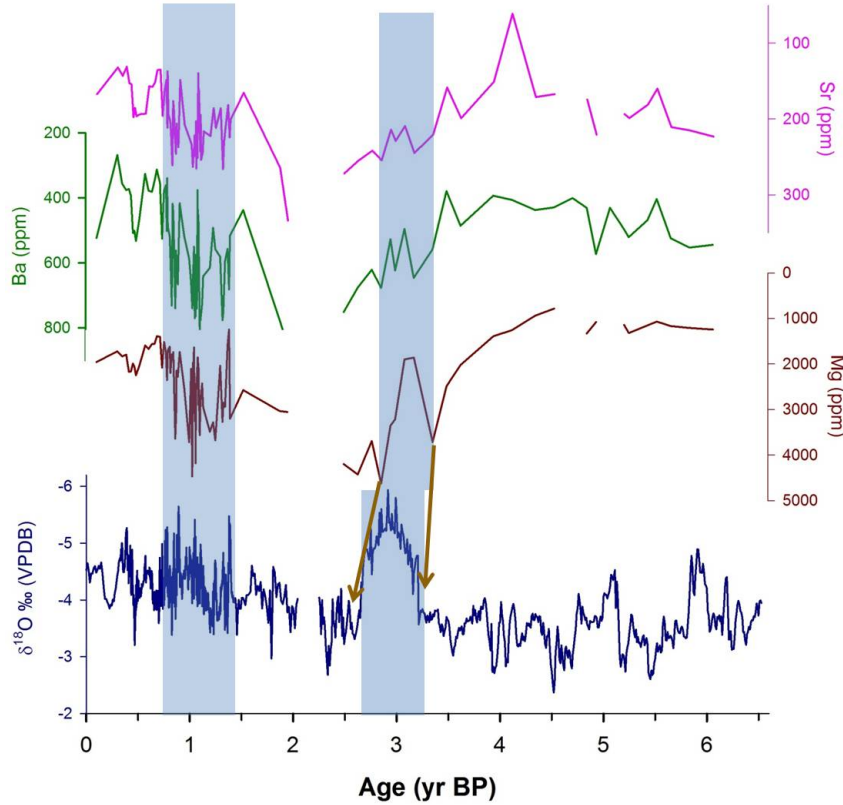
Figure 4.5: *Trace element variations in the Dan-I speleothem. Concentrations of Magnesium (Mg, Red),Barium (Ba,Green) and Strontium (Sr,Pink) are reported in ppm. The trace element profiles are compared with the $\delta^{18}O$ values (blue). The arrows point to the peak in trace element with the corresponding $\delta^{18}O$ variability. Shaded regions show the zones of similar variability observed in the trace element and $\delta^{18}O$ data.*

4.2 The Dandak-II stalagmite

4.2.1 U-Th ages

The timeseries of the Dandak-II stalagmite is based on four U-Th ages for a length of 41.3 cm of the sample (Table 4.2). The ages have overlapping errors, hence no outliers were detected. The age model was reconstructed using COPRA with 3000 Monte Carlo simulations (Figure 4.6). The errors are reported as 2σ values and the confidence interval of 95% is shown in red dashed lines. Corrected ages

use an initial $^{230}Th/^{232}Th$ atomic ratio $= 0.0012 \times^{232} Th^{-0.6386}$ where, ^{232}Th is concentration in parts per million (ppt), with the supposition that lower concentration of ^{232}Th equate to higher $^{230}Th/^{232}Th$ ratios. Years before present $=$ yr BP, where present is AD 2007. Subsamples weighing $\sim 90 - 408$ mg were used. The Dandak-II stalagmite spans from 10.4 - 9 ka and shows a steady growth rate of $\sim 0.4\ mm/yr$.
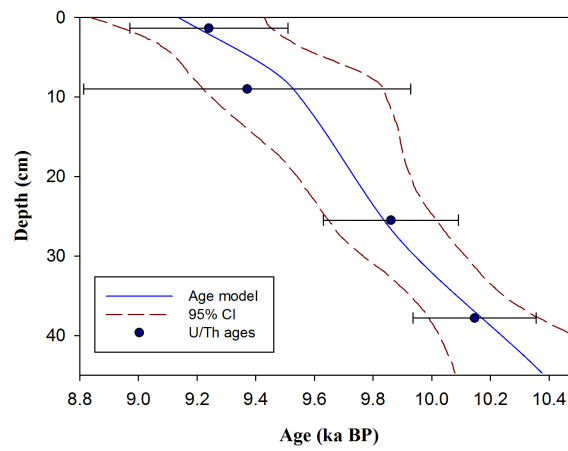

Figure 4.6: *Age model for Dan- II stalagmite reconstructed using COPRA-interactive program on MATLAB [Breitenbach et al., 2012]. The filled blue circles are ^{230}Th ages taken for age model. The errors are reported in 2σ. The dashed lines show 95% confidence interval and the blue lines are the median through which the age model passes.*

4.2.2   Stable isotopes of oxygen and carbon

A total of 2250 subsamples from the Dandak-II stalagmite were analyzed on a Delta-V plus IRMS. The $\delta^{18}O$ and $\delta^{13}C$ timeseries are shown in Figure 4.7. The sample shows a gradual -5‰ decrease in the $\delta^{18}O$ from 10.4 to 9 ka. This steady depletion is however punctuated by a cluster of sharp ^{18}O enriched peaks occurring at regular intervals.The $\delta^{13}C$ values vary between -2 to -8‰, with the values fluctuating around the mean of -3.5‰. The $\delta^{13}C$ data do not necessarily mimic the $\delta^{18}O$ profile. However, the peaks in the $\delta^{18}O$ values are also observed in $\delta^{13}C$ (Figure 4.7).

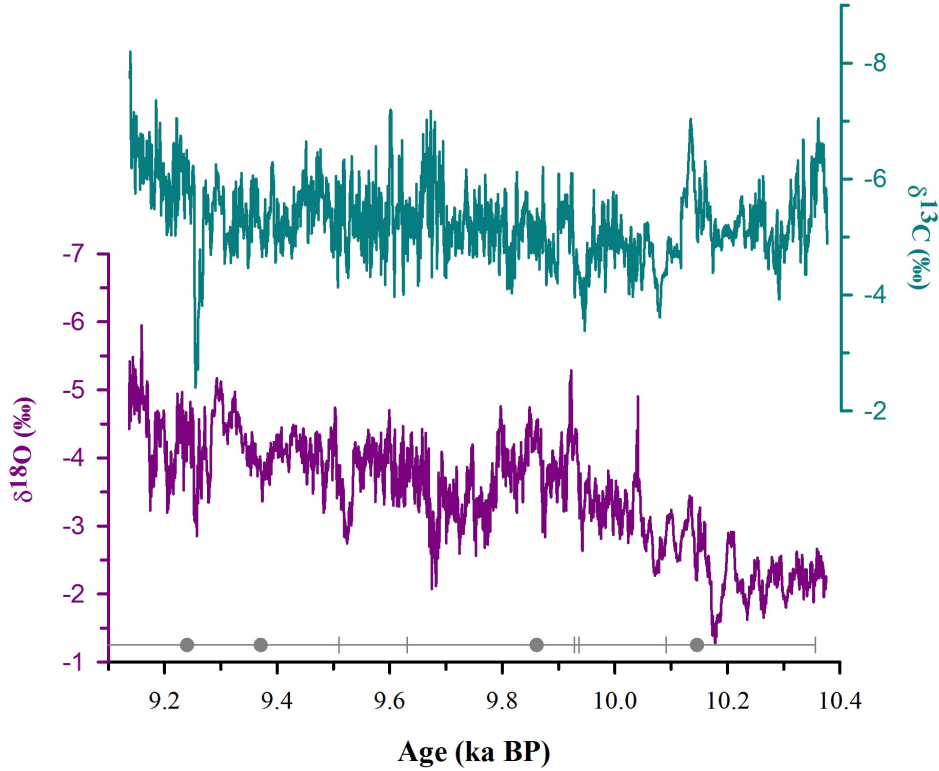**Figure 4.7:** $\delta^{18}O$ *(Purple) and $\delta^{13}C$ (cyan) profiles of Dandak-II stalagmite. The timeseries represents the profile based on ages derived from Copra age model. The ages considered in the model are shown as gray filled circles. The errors are reported in 2σ*

4.2.3   Hendy's test

As seen in Figure 4.8, there is no significant enrichment of ^{18}O and ^{13}C along the layers. Also, there a poor correlation between $\delta^{18}O$ and $\delta^{13}C$ values. This implies that there was minimal evaporation and slow degassing during the deposition of calcite otherwise the precipitating calcite would undergo kinetic fractionation and would show enrichment in ^{18}O along the tapering ends of a layer. This ensures that the sample was precipitated under isotopic equilibrium.
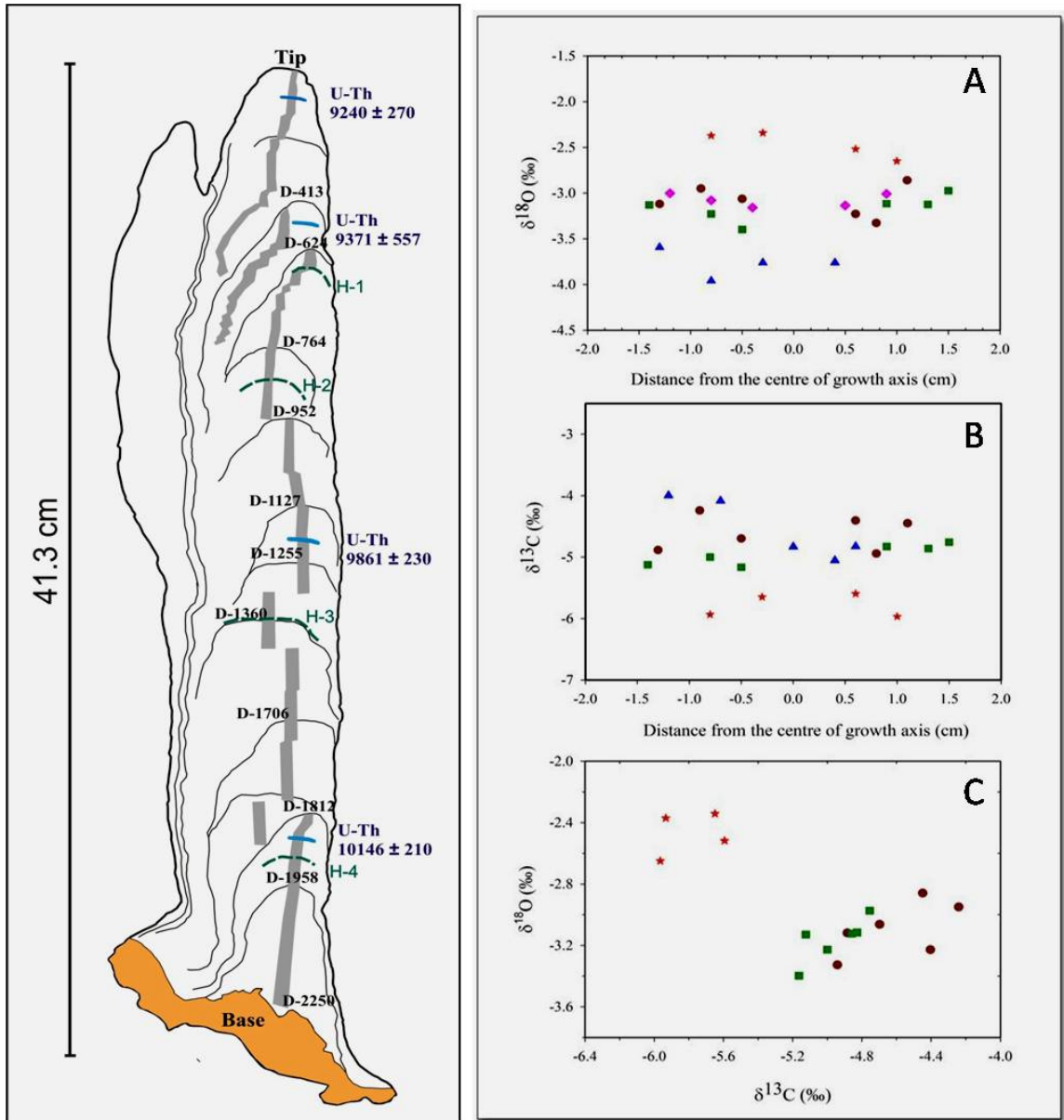
Figure 4.8: *Left:Sketch of the Dandak-II stalagmite, showing sampling the sampling sites for Hendy's test(dashed green) and U-Th ages(dark blue) Right: (A) and (B) $\delta^{18}O$ and $\delta^{13}C$ variability along four layers. (C) The correlation between $\delta^{18}O$ and $\delta^{13}C$ used to indicate isotope equilibrium between precipitating calcite.*

4.3   Kotumsar stalagmite

4.3.1   U-Th ages

The U-Th ages for the KOT-I stalagmite were obtained from the National Taiwan Unviersity.Table 4.3 shows the 15 ages with associated errors. The sample has many reversals and non-tractable outliers. The reversals with very old ages occur when there is a post-depositional U loss from the sample giving artificially old ages. Some reasons for the loss can be a sample that has been recrystallized from aragonite to calcite or perhaps flooding immediately after deposition (which could also cause recrystallization). These reversals were removed from the age models. The sample as seen in Figure 3.5 has a band of high detrital content and high ^{232}Th values. Thus, the ages in this band show reversals and are unreliable.The age model was then constructed based on 6 ages, and is shown in Figure 4.9. The growth of the sample is from $\sim 8.4 - 5.6$ ka BP. The rate of growth however, has varied during its course of deposition, from 8.4 -6.5 ka BP, the deposition rate was slow at ~ 0.055 mm/yr. The stalagmite growth was rapid between 6.5-5.6 ka BP, with the rate of ~ 0.23 mm/yr.

4.3.2   Hendy test

The results of Hendy test performed on four layers of KOT-I sample are shown in Figure 4.10. The $\delta^{18}O$ values along a layer do not show major fluctuations and also there is a poor correlation between $\delta^{18}O$ and $\delta^{13}C$ values. This ensures that the sample was precipitated under an isotopic equilibrium and can be used for paleomonsoon reconstructions.
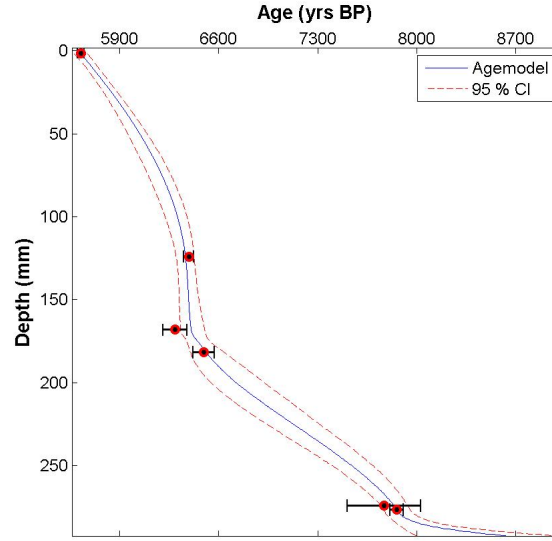
Figure 4.9: *Age model for the Kotumsar stalagmite using the COPRA- interactive program on MATLAB [Breitenbach et al., 2012]. The filled blue circles are ^{230}Th ages assumed for the age model. The errors are reported in 2σ. The dashed lines show 95% confidence intervals and the blue line is the median through which the age model passes.*
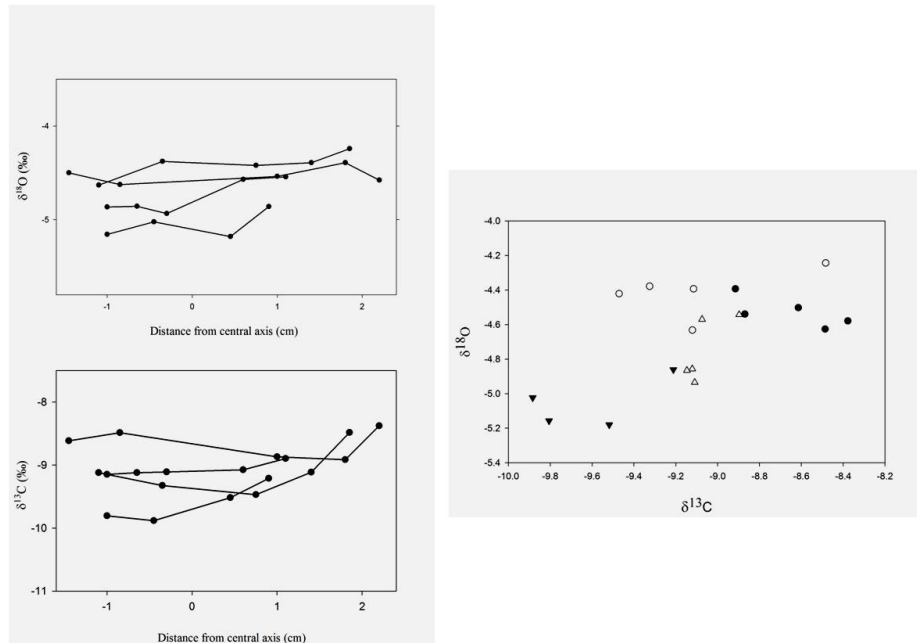

Figure 4.10: *Left: Top $\delta^{18}O$ and Bottom $\delta^{13}C$ variability along four layers is plotted. Right: The correlation between $\delta^{18}O$ and $\delta^{13}C$ is used to indicate deposition of calcite under isotopic equilibrium.*

4.3.3 Stable isotopes of oxygen and carbon

The stable isotope ratios of oxygen and carbon are shown in Figure 4.11. The $\delta^{18}O$ values vary between -6 to -3‰, with fluctuations around a mean of -4.5‰. The oxygen and carbon data show dense points between 7.5 - 5.6 ka BP. This is owing to the age model, where the regularly spaced proxy record has been squeezed intoa precise time frame.The values show a decreasing trend from 6.5 - 5.6 ka BP. This could be attributed to an increase in rainfall, which was also seen as increased growth rates for this section of the sample. The oxygen data also shows episodes of periodic ^{18}O enrichment. The $\delta^{13}C$ profile covaries with the $\delta^{18}O$ values. The remarkable decreasing trend from 6.5 - 5.6 ka ia also observed in $\delta^{13}C$ record. The episodes of ^{13}C enrichment replicate the corresponding dips in $\delta^{18}O$ values. Hence, we can assume that, $\delta^{13}C$ values of this stalagmite, respond to climate changes, and hold a potential for paleomonsoon reconstruction.

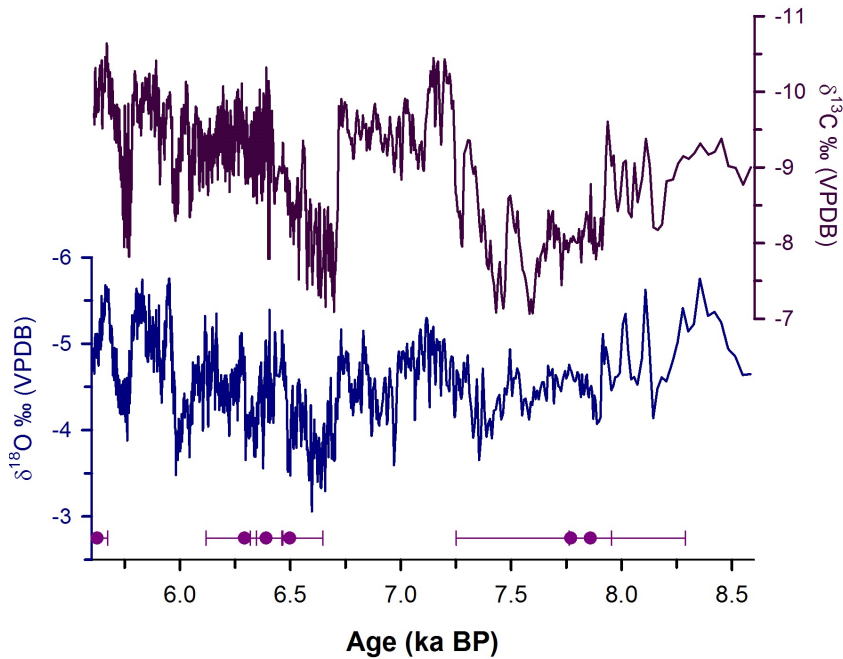**Figure 4.11:** *$\delta^{18}O$ (dark blue) and $\delta^{13}C$(purple) timeseries of KOT-I stalagmite. The stalagmite was deposited between 8.4-5.6 ka BP. The ages considered in the model are shown as pink filled circles. The errors are reported as 2σ.*

4.4 Tree Rings

In tropical regions of south and southwest Asia, good tree-ring data networks have been established to document monsoon variability. In this context, teak (*Tectona grandis*) from Indonesia, Thailand, Java and India have been demonstrated as a potential source for high resolution reconstruction of ISM [*Bhattacharyya et al.*, 1992; *Borgaonkar et al.*, 2010; *Buckley et al.*, 2007; *D'Arrigo et al.*, 1994; *Jacoby Jr et al.*, 1990; *Murphy et al.*, 1989; *Pant and Borgaonkar*, 1983; *Pumijumnong et al.*, 1995; *Shah et al.*, 2007].
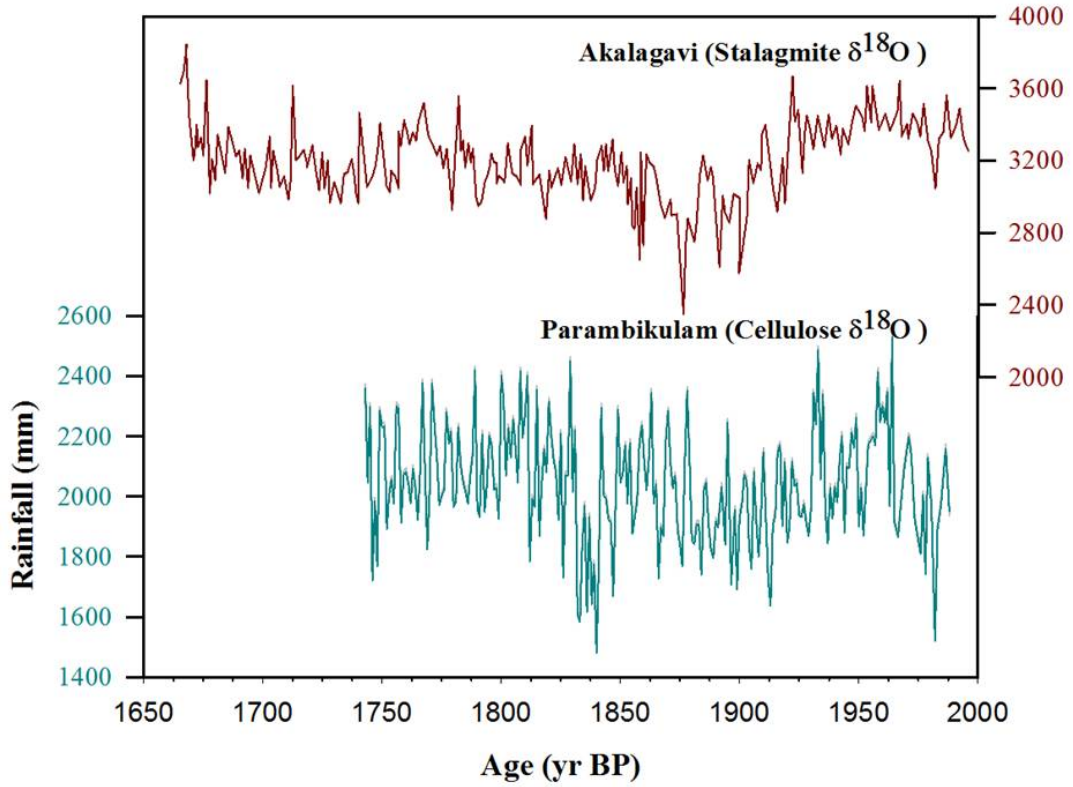

Figure 4.12: *Monsoon rainfall reconstructed from Ulvi speleothem (top, Yadava et al. [2004]) and Parambikulam teak cellulose (bottom, Managave et al. [2011a]). Solid curves show the reconstructed values.*

Managave et al. [2010, 2011b] showed that high resolution intra-ring analysis of $\delta^{18}O$ of cellulose from several annual growth rings of teak trees was very much useful in achieving a ~ 20 day resolution in the monsoon reconstruction. *Ramesh et al.* [1989] reported the correlation of stable isotopic ratio of hydrogen (δD) in teak with the amount of rainfall and mean maximum temperature to demonstrate its applicability for reconstruction of past climate. The lower panel of 4.12 shows the monsoon reconstruction for Parambikulam, Kerala for more than 2 centuries in the past (Managave et al., 2011). This can be compared with the three century long monsoon reconstruction for northern Karnataka (top panel of the same 4.12, locations shown in Figure 4.13) based on $\delta^{18}O$ variations in a stalagmite that had annual resolution.

4.5   Oceanic records

Contrary to terrestrial deposits, marine deposits preserve a more complete and continuous monsoon record. Extensive studies has been carried out on the evolution of the monsoon through the Holocene [*Sirocko et al.*, 1993; *Tiwari et al.*, 2011] using marine sediments. $\delta^{18}O$ variations recorded by foraminifera in marine sediment cores from the eastern Arabian Sea have shown a consistent increasing trend in the monsoon rainfall [*Sarkar et al.*, 2000] during the Holocene. Figures 4.13 and 4.14 shows locations and monsoon reconstruction from six sediment cores of Arabian sea.

All the oceanic records show consensus that there is a prominent reduction in the $\delta^{18}O$ values between $\sim 11 - 10$ ka BP. Core SK148/4 [*Rao et al.*, 2010] shows an abrupt enrichment between $\sim 8 - 4$ ka BP, while similar abrupt changes are observed in Core 3268G5 at 6 ka BP. The shaded gray regions in Figure 4.14 are Bond events in the Holocene numbered from 0 to 8. The event 3 by far is one of the most important and large event and is witnessed as a sharp enrichment in ^{18}O in 3268G5 and SK148/4 cores. In the rest of the cores, some discrepancy in

the trend exists, while event 1 famously known as the Little Ice Age is recorded in almost all the cores.

Although continuous, marine sediment cores lack the resolution to be able to distinguish small climate changes. And hence in this study the results from such sediment cores are to check for high amplitude variations in climate and study the evolution of monsoon on a millennial timescale.
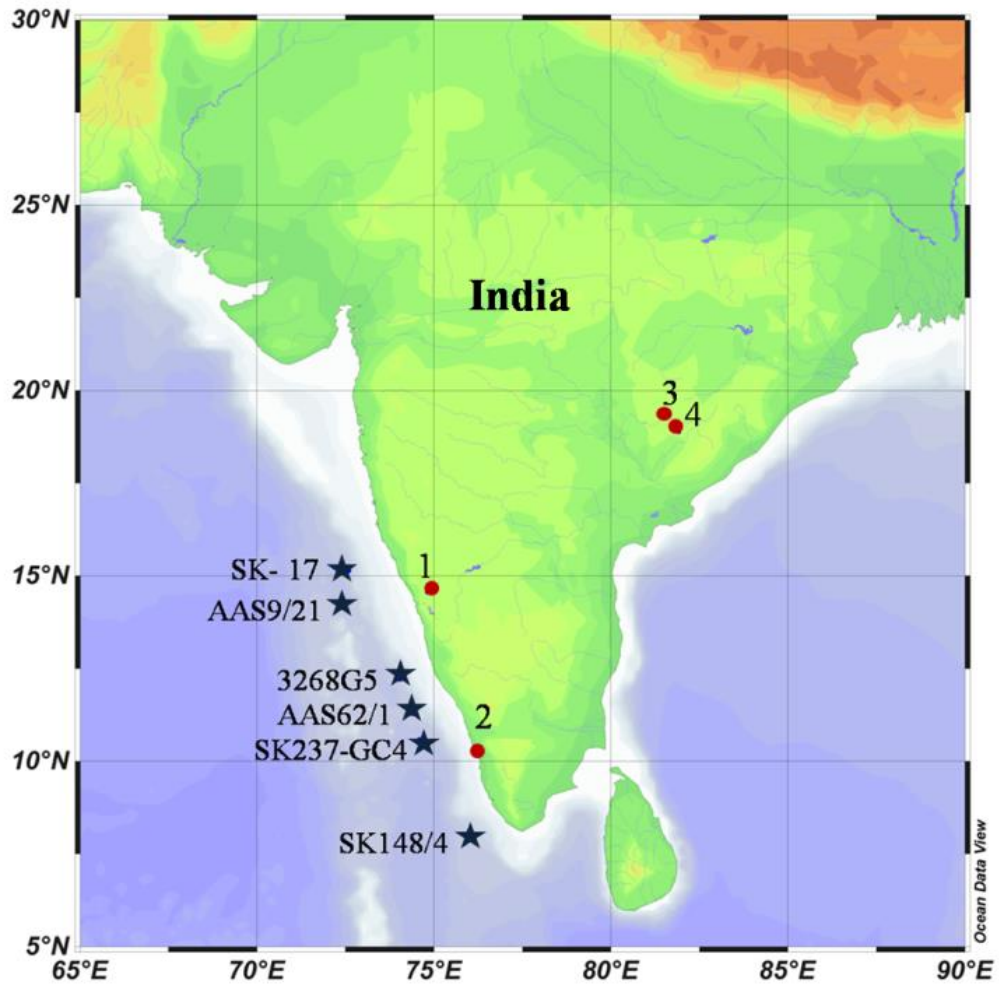

Figure 4.13: *Locations of marine and terrestrial proxies. Stars are sediment cores.Core SK-17 [Singh et al., 2006], Core AAS9/21 [Govil and Naidu, 2010], Core 3268G5 [Sarkar et al., 2000], Core AAS62/1 [Kessarkar et al., 2013], Core SK237-GC4 [Saraswat et al., 2013], and Core SK148/4 [Rao et al., 2010]. Terrestrial proxies are (1) Akalagavi cave stalagmite [Yadava et al., 2004], (2) Parambikulam tree cellulose [Managave et al., 2011b], (3) and(4) are speleothems from the Dandak and Kotumsar caves [Yadava and Ramesh, 2005].*
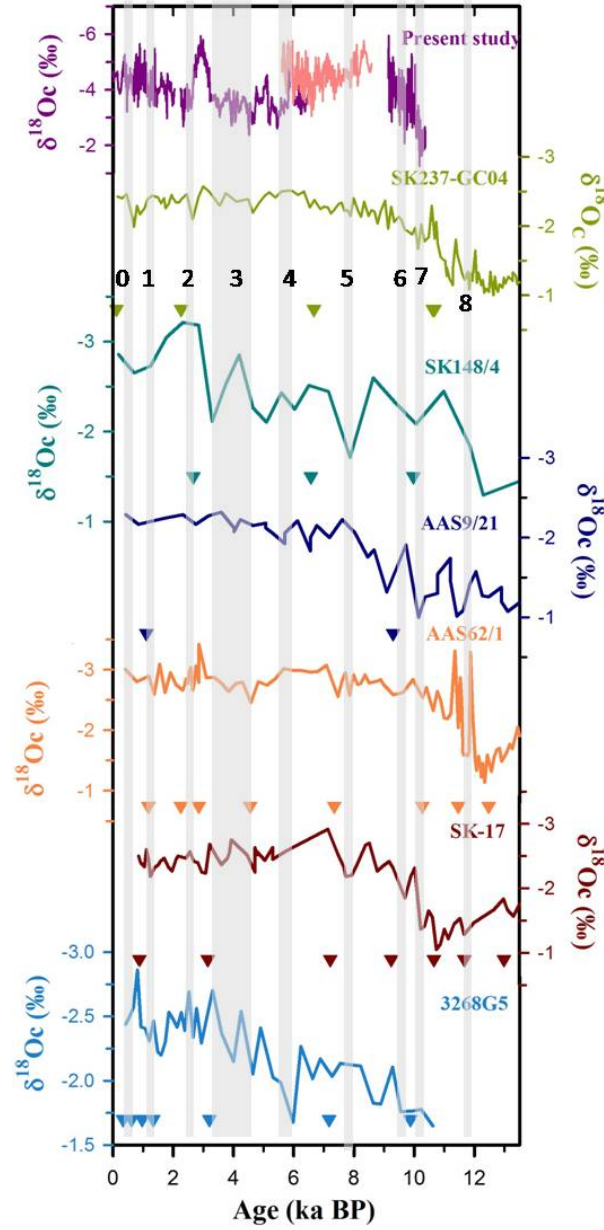
Figure 4.14: $\delta^{18}O$ *variations of planktic foraminifera from six different cores from the eastern Arabian Sea (See Figure 4.13 for locations) during the Holocene, plotted with error bars (gray shaded regions). Inverted triangles represent ^{14}C ages of planktonic foraminifera from the respective cores. The sediment core records are compared with reconstructed monsoon variability from the Dandak(Pink) and the Kotumsar cave (light pink) stalagmites. Sources: (Rao et al. [2010], Cyan),(Saraswat et al. [2013], Green), (Govil and Naidu [2010], Dark blue),(Kessarkar et al. [2013], Orange),(Singh et al. [2006], Maroon),(Sarkar et al. [2000], light blue) Shaded gray regions are Bond events during the Holocene, numbered from 0 to 8 [Bond et al., 2001].*

4.6 Discussion

A few speleothem studies around India vis-a-vis Qunf cave, and caves in China were used to explain the variability in ISM during the Holocene. So far, terrestrial records from the core monsoon region of India were fragmented and hence addressing the monsoon variability from the Indian region proved to be a challenge. On the other hand Chinese speleothems were used to reconstruct east Asian monsoon variability and establish a link between the climate changes at the high and low latitudes. However, more recently *Pausata et al.* [2011] based on the general circulation model postulated that chinese speleothem $\delta^{18}O$ excursions reflect changes in Indian Summer Monsoon than Heinrich events [*Johnson*, 2011]. The sensitivity test carried by *Pausata et al.* [2011] showed that Heinrich events led to cooling in northern Indian ocean and reduced the convective precipitation. As a result isotopically enriched moisture was carried across India and moisture rich in $\delta^{18}O$ were also carried over China. Accordingly, the positive excursion in the Chinese speleothems reflect variations in $\delta^{18}O$ value of moisture exported from India. *Pausata et al.* [2011],also suggests that speleothems from India are ideal for paleomonsoon reconstructions whereas, Chinese speleothems seem to record changes in the isotopic composition of the incoming water vapor. Considering that the Indian ocean plays a key role in precipitation over India and East Asia during June-August, the above postulation may hold true.

Hence it is extremely important to study Indian speleothems to reconstruct Indian monsoon and to understand the role of North-Atlantic circulation changes as one of the governing factors. With this as an objective, we have attempted to reconstruct high resolution ISM variability from CMZ of India. Our high resolution record from the Kotumsar and Dandak cave together, have provided monsoon record from ~ 10.5 ka - to the present with a brief hiatuses between $\sim 9 - 8.5$ ka BP and $\sim 2.2 - 2$ ka BP. The $\delta^{18}O$ profile is constructed using ~ 5040 subsamples and 15 U/Th ages.

The record extends from ∼ 10.4 ka BP to the present. An overlap of the Kotumsar and Dandak- I profile between 7-6 ka BP. The region of overlap shows similar trend in monsoon. Our speleothem record, when compared with available monsoon records reconstructed from speleothems from Oman and China indicate, changes in Asian monsoon system comprising of ISM and EASM have similar variability. The caves which are in two seperate domains of Asian monsoon, show similar trend in monsoon variability, proving it to be a robust climate signal.
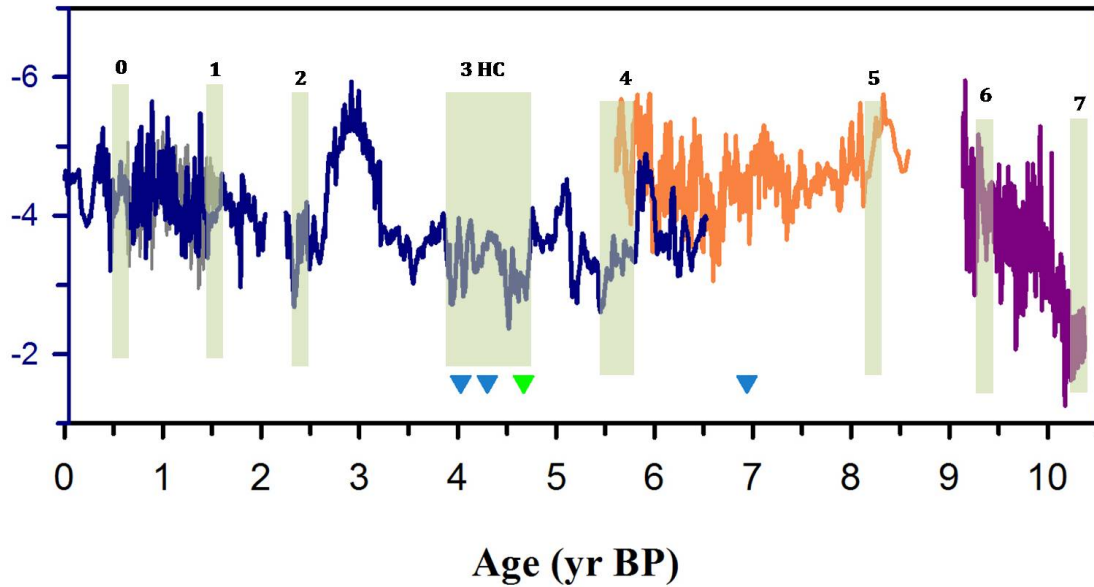

Figure 4.15: *Compiled Holocene monsoon record based on $\delta^{18}O$ variability in KOT-I, Dandak-I and II stalagmites. Blue and green triangles are the radiocarbon dates of charcoal derived from the Kotumsar and the Dandak caves, respectively. The green shaded regions are North Atlantic cooling events, known as 'Bond Cycles'. The event numbered 3, marks the culmination of the Harappan Civilization (HC)[Giosan et al., 2012].*

4.6.1 Early Holocene climate (∼ 10.4 - 8 ka BP)

The inception of the Holocene marks the rapid intensification of monsoon between 10.4 - 9 ka BP. Stronger monsoon is observed as a rapid decrease in $\delta^{18}O$ (around 5‰ depletion) values, and the record has a brief hiatus between ∼ 9−8.5

ka BP (Figure 4.15). The strength of monsoon is also seen as a faster growth rate of the Dandak-II stalagmite. The increased monsoonal conditions were related to the Northward shift of ITCZ between $\sim 10.5 - 5.4$ ka BP, owing to the seasonality in the 21 ka precession cycle [*Haug et al.*, 2001]. By 11-10 ka BP, the insolation over the Northern Hemisphere rose 8% greater than today due to orbital precession that gradually aligned the boreal summer solstice with the perihelion [*Ortiz et al.*, 2000]. This early increase in the boreal summer radiation enhanced monsoonal circulation, which is also witnessed in the present study, and other available paleoclimate records (eg. [*Foley et al.*, 1994; *Haug et al.*, 2001]) also deduced from climate models [*Prell and Kutzbach*, 1987]. This record is in agreement with other speleothem records [*Burns et al.*, 2001; *Neff et al.*, 2001], Arabian Sea upwelling records [*Overpeck et al.*, 1996; *Sirocko et al.*, 1993] ice core data [*Thompson et al.*, 1989], and lake levels from India [*Enzel et al.*, 1999]. Comparison between the Qunf cave, Dandak-II and the GRIP ice core record (Figure 4.16) shows an increase in monsoon is in phase with the increase in the North Atlantic atmospheric temperature. Considering the error limits on the ages of the Dandak-II stalagmite, the cold events recorded in the GRIP core are witnessed as reduced monsoon precipitation at ~ 10.3 and 9.4 ka. This establishes a strong teleconnection between low and high latitude temperature changes. Contemporaneous changes in climate were observed in Africa, where the strength of eolian deposition reduced significantly [*Ortiz et al.*, 2000]. This time period is known as African Humid Period.

An abrupt increase in the monsoon was observed between $\sim 10 - 9.5$ ka BP in several other marine sediment cores (Figure 4.14) from the eastern Arabian Sea [*Govil and Naidu*, 2010; *Kessarkar et al.*, 2013; *Overpeck et al.*, 1996; *Rao et al.*, 2010; *Saraswat et al.*, 2013; *Sarkar et al.*, 2000; *Singh et al.*, 2006]. The increasing trend of monsoon rainfall during the Holocene is also confirmed by $\delta^{18}O$ variations in speleothems from Central India [*Yadava and Ramesh*, 2005]. Our record is correlatable with the Sanai lake record from Ganga plains. Both

these records agree with climatic optimum at $\sim 10.4 - 6$ ka witnessed by lake expansion and high prevelance of aquatic plants [*Sharma et al.*, 2004].
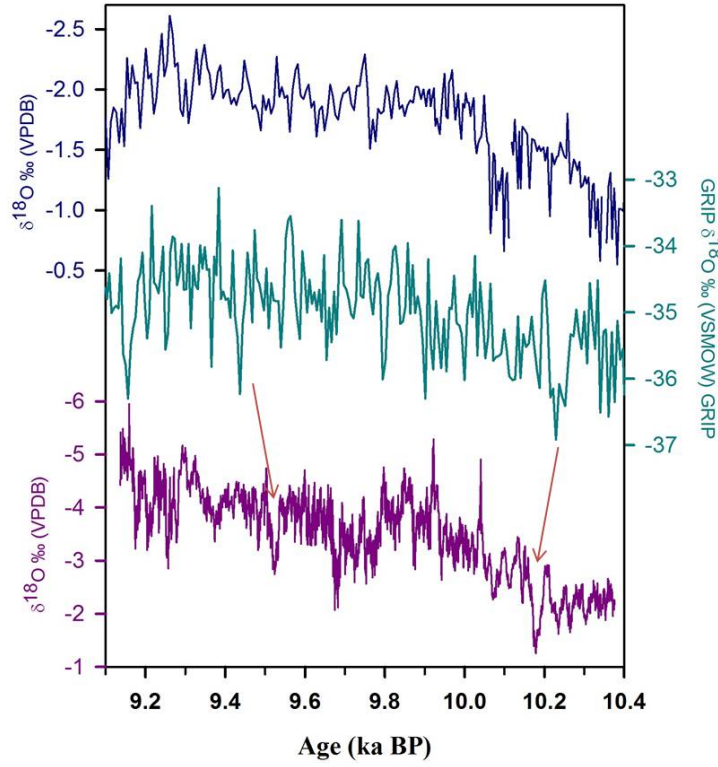

Figure 4.16: *Comparison between Dandak- II stalagmite(Purple), GRIP ice core record(cyan, Dansgaard et al. [1993]) and Qunf cave(blue, Fleitmann et al. [2003].)*

4.6.2 Mid- Holocene climate ($\sim$ 8 - 4 ka BP)

Climate during the mid-Holocene was observed to change significantly. During this time air temperatures on land declined globally, the evidence of which is recorded clearly in ice cores (Greenland, Antarctica and eastern Canadian arctic) [*Steig et al.*, 1998]. In low latitudes the temperatures were lower or they experienced aridity. At many places, abrupt change in climate during the mid-Holocene is documented. In addition to temperature and precipitation changes, the mid-Holocene also experienced change in atmospheric and ocean circulation. To-

gether with these changes, the climate during this period was very different from the present conditions. *Steig* [1999] stated that Mid-Holocene climate changes are more complex and require high-resolution, high-quality studies from different localities. These changes are attributed to a steep decline in the Northern Hemisphere insolation at $\sim$ 6 ka BP [*Charles et al.*, 1996; *Wright*, 1993]. Climatic events between 6000-5000, 4200–3800, 3500–2500 and 1200–1000 cal years BP were classified under "cool poles, dry tropics"pattern by *Mayewski et al.* [2004].

The monsoon intensity gradually decreased between 8 to 6 ka, the owing to southward shift of ITCZ and decreasing [*Fleitmann et al.*, 2003; *Haug et al.*, 2001; *Paillard et al.*, 1996] June-August insolation at 30°N. When the ITCZ shifts southwards, the land-sea temperature contrast deceases, leading to weakening of the monsoon. Weaker monsoon is also recorded in the Arabian Sea sediment core $\delta^{18}O$ values of *G.ruber* [*Singh et al.*, 2006] and abundances of *G.bulloides* [*Gupta et al.*, 2003] and in the lake records of Garhwal [*Srivastava et al.*, 2013]. The migration of ITCZ is also observed to affect the East Asian Summer Monsoon (EASM), the second domain of Asian monsoon, as recorded in the Dongge cave speleothem. The mid-Holocene witnessed widespread aridity in all the Asian monsoon domains [*Dykoski et al.*, 2005; *Fleitmann et al.*, 2003; *Sharma et al.*, 2004; *Wang et al.*, 2005]. A few studies report the onset of aridity as a gradual mechanism [*Fleitmann et al.*, 2003, 2007; *Gupta et al.*, 2003; *Ivanochko et al.*, 2005; *Overpeck et al.*, 1996; *Wang et al.*, 2005], while others infer it to be an abrupt event [*Anderson et al.*, 1988; *Gasse and Van Campo*, 1994; *McClure*, 1976; *Morrill et al.*, 2003; *Sarkar et al.*, 2015]. Our record shows, an abrupt decrease in the monsoon between $\sim 6 - 3.5$ ka BP, with the driest period between $\sim 4.7 - 4$ ka BP (Figure 4.15). *Fleitmann et al.* [2003], who are in favor of a gradual decline, have argued that the abrupt signal recorded in the African and Indian monsoon proxies is on account of nonlinear response of ISM. High-amplitude fluctuations in the monsoon precipitation may induce sudden negative precipitation minus evaporation(P-E) balance, leading to the drying of a lake. This argument may

hold true, for the lake records, however, speleothems from core ISM regions are less susceptible to such changes and are likely to preserve a better climate signal. *Morrill et al.* [2003], on the other hand believe that such abrupt changes in the monsoon are due to abrupt events in the external forcings or in natural or internal fluctuations of the monsoon system. External forcings including insolation and volcanic eruptions, whereas internal fluctuations include the North-Atlantic thermohaline circulation and El-Nino. During the Holocene, a gradual decrease in insolation is observed and hence can not be the sole factor in controlling the monsoon. *Turney et al.* [2005], concluded that centennial to millenial changes in the North Atlantic Climate are not solely driven by insolation. Hence the abrupt decrease in monsoon may have two possible influences. The first being the abrupt change in the North-Atlantic thermohaline circulation. The sensitivity of monsoon system to the North Atlantic changes is evidenced as effect of the short term Bond events on the weakening of the ISM. And the second plausible explanation could be sudden failure of internal feedback mechanisms governing monsoon leading to a sudden decline in the monsoon intensity. The factors governing abrupt changes in ISM in the core monsoon region of India, requires further investigation. *Ortiz et al.* [2000] and *Claussen et al.* [1999], explained such abrupt changes observed in the African monsoon as occurring due to vegetation-albedo positive feedback amplifying the insolation-driven changes in the monsoonal climate.

Our record shows a close resemblance to the High resolution Holocene precipitation from the stalagmites from the Qunf cave, Oman [*Fleitmann et al.*, 2003], the Dongge cave, China [*Dykoski et al.*, 2005; *Wang et al.*, 2005], titanium concentration record from the Carioaco basin [*Haug et al.*, 2001], suggesting role of shift of ITCZ in controlling the low-latitude climate variability (Figure 4.17). The intensity of monsoon over India increased post 3.5 ka.

When sampling, evidences of controlled fire preserved as burnt earth and patches of charcoal mixed with soil and grasses in the form of three distinct layers in the Kotumsar and one layer in the Dandak cave were found [*Yadava and*

Ramesh, 2007]. Such deposits indicate sporadic human inhabitance. Radiocarbon dating of these layers narrow down such possible human activity to be between $\sim 6.9-4$ ka BP in the Kotumsar cave and ~ 4.6 ka BP in the Dandak cave(Figure 4.18). The samples were studied under a stereo binocular microscope and three grasses and two millet species were identified by previous workers [*Yadava et al.*, 2007]. The grasses were *Cenchrus L, Celosia argentea L.* and *Panicum L* and the millets were identified as foxtail. By the mode of preservation, it can be inferred that millets were important for the sustenance of the Kotumsar cave-dwellers. Millets are drought tolerant crops, and suitably grow in low rainfall regions. Archaeo-biological researches carried out at 45 archaeological sites in India have revealed that millet cultivation began as early as 5.3 ka BP [*Pokharia et al.*, 2014]. The radiocarbon ages of the charcoal deposits fall in the same range as that of the formation of KOT-I and Dandak-I stalagmites, suggesting that the caves were used as shelters during severe droughts. During one of the visits made to the Kotumsar cave in CE 2000 (wet season), it was observed that the cave entrance was inaccessible as the rain water was gushing out through the cave mouth. However, the entrance was dry and accessible during the pre-monsoon and winter. As seen in Figure 4.18, the strength of the monsoon declined between $\sim 6-3.5$ ka. The drought like conditions would have made caves accessible during these periods. Based on this, it can be postulated that the caves were used as a temporary dwelling and food storage site, during the weaker/drier phases of monsoon. Widespread aridity is also considered as a reason for the collapse of contemporaneous major civilizations like the Harappan, Chinese and Mesopotamian. Evidence of Indus valley suggests that, as the intensity of ISM decreased significantly, from ~ 5 to 4 ka (~ 6 to 3.5 ka, in the present study), the type of agriculture shifted towards Kharif (summer) crops, and drought tolerant crops such as millets [*Clift et al.*, 2012; *Giosan et al.*, 2012; *Weber and Belcher*, 2003].
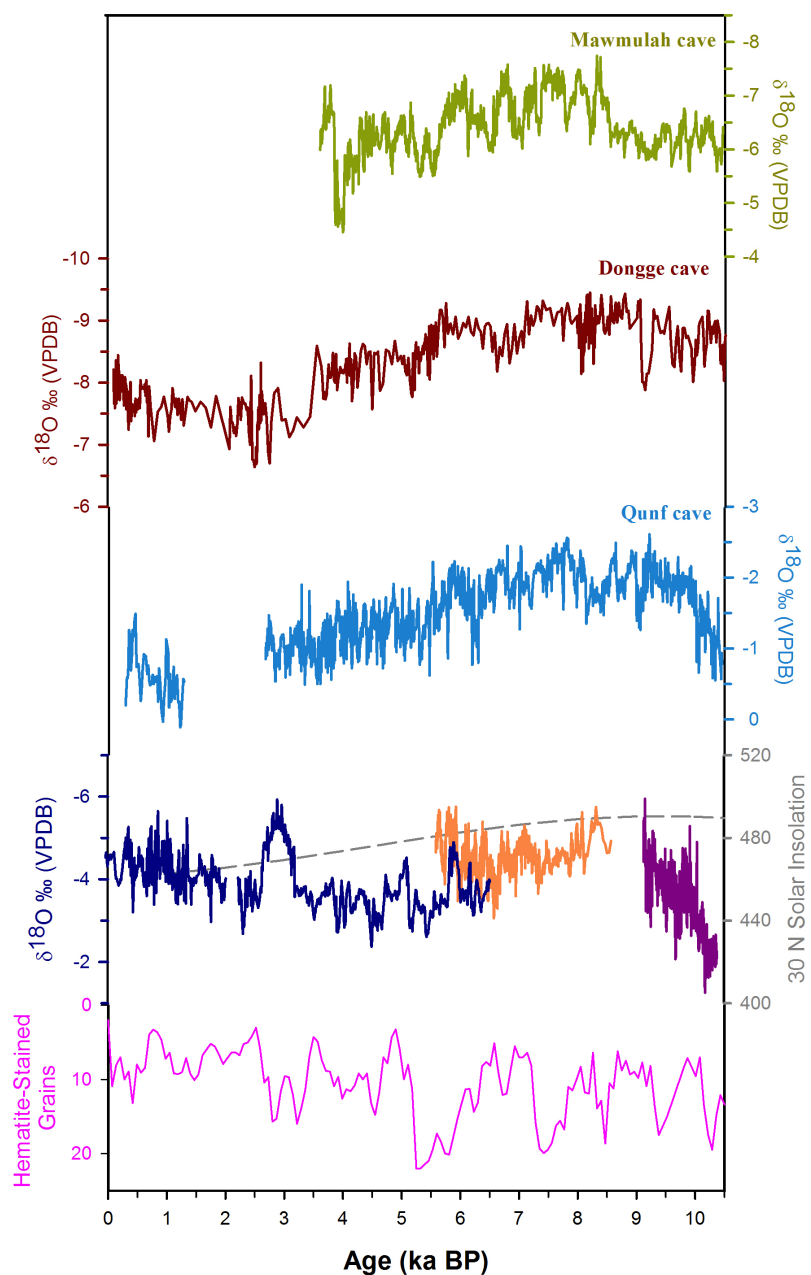
Figure 4.17: *$\delta^{18}O$ records of the Mawmulah cave(Green,Berkelhammer et al. [2012]), the Dongge cave (red,Dykoski et al. [2005]), the Qunf cave (blue,Fleitmann et al. [2003]),the present study(Dark blue), and hematite-stained grains(pink, Bond et al. [2001]).*
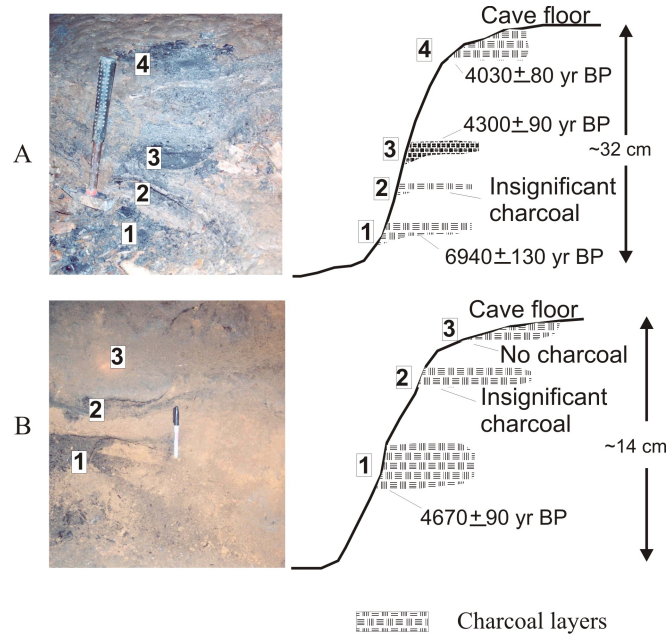
Figure 4.18: *Charcoal layers preserved in sediments of Kotumsar cave (A) and Dandak cave (B) Photo taken from* Yadava and Ramesh [2007].

4.6.3 Late Holocene climate (~ 4 - to the Present day)

According to the observations made by Ponton [2012]; Ponton et al. [2012] and Sarkar et al. [2015] the monsoon intensity decreased from 4.8 ka - to the present. Their interpretation is based on $\delta^{13}C$ of leaf wax and interpreted in terms of C3/C4 type of vegetation, whereas, all other records [Breitenbach, 2010; Chauhan et al., 2010; Fleitmann et al., 2003; Govil and Naidu, 2011; Staubwasser and Weiss, 2006], including the present study, are based on interpreting $\delta^{18}O$ values of proxies which are direct recorders of monsoon. These records show consensus that monsoon increased post 2 ka BP. Speleothem studies from Socotra island, show a depletion of 2‰ from ~ 4 ka to the present, implying that the monsoon increased during late Holocene [Fleitmann et al., 2007]. As seen in Figure 4.15, $\delta^{18}O$ record between 3.8 - 2.8 ka BP is anomalously depleted, a feature not seen in other records. The effect of moisture source change from Arabian Sea to the Bay of Bengal, causes a depletion of ~ 1‰ and therefore is insufficient to explain

the $\sim 2.5‰$ decrease in $\delta^{18}O$ values. Hence, this can either be explained as a local intensification of monsoon or an effect of both these parameters. Figure 4.19 shows reconstructed ISM for the last 2000 years. These records are compared with annually deposited Jhumar [*Sinha et al.*, 2011] and Dandak [*Sinha et al.*, 2007] speleothem records. The sharp troughs recorded in our study correspond to the troughs in Jhumar speleothem at a different time interval. This shift is mainly due to the different age models used to reconstruct the data. The age model for Jhumar cave is reconstructed based on counting of annual layers, whereas our age model was reconstructed based on U-Th ages with associated errors. However, barring this small shift, the monsoonal trends in both the records covary and record major climate events.

Two most important climate events of the early Holocene were the Medieval Warm Period and the Little Ice Age, affecting most of Europe. These high latitude climate changes also affected tropical ocean surface temperature and the monsoon rainfall [*Newton et al.*, 2006]. Based on historical records,the most recent cooling period in the Holocene known as the 'Little Ice Age' occurred as two discrete events [*Jones*, 1995]. High resolution Greenland ice core $\delta^{18}O$ records reconstructing surface temperatures, suggest the occurrence of these discrete events centered at $\sim$1500 and 1850 A.D [*Dahl-Jensen et al.*, 1998]. Our record shows evidence of these events as abrupt decline in monsoon between 1550-1450 AD and 1350-1250 AD(as shown in Figure 4.19 with arrows). Corresponding ^{18}O depletion is also observed in the Jhumar cave $\delta^{18}O$ record. *Sinha et al.* [2007] have inferred a 30% reduction in rainfall in 14th century. Historical records during this period report several famines and droughts. The major documented drought events coincide (within the dating uncertainty) with a period of reduced rainfall reconstructed from the Dandak stalagmite [*Maharatna*, 1996; *Pant et al.*, 1993]. The Durga Devi famine (1396 A.D. to 1409 A.D.) [*Maharashtra-Government*, 1973] coincides with the first positive excursion of LIA. Multiproxy records from the Arabian Sea sediment cores [*Agnihotri et al.*, 2002; *Gupta et al.*, 2003; *von*

Rad et al., 1999], Stalagmite $\delta^{18}O$ [*Burns et al.*, 2002; *Fleitmann et al.*, 2007] records of Oman and Yemen also indicate a weaker monsoon during LIA and a stronger monsoon during MWP.
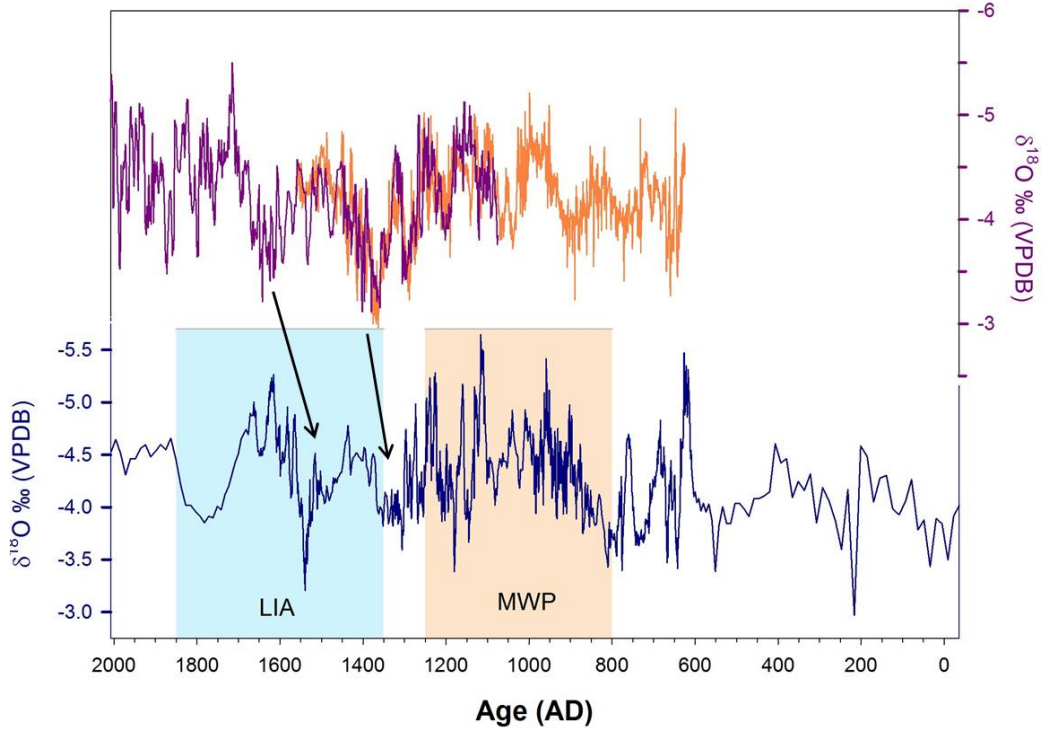

Figure 4.19: *The $\delta^{18}O$ time series of Jhumar speleothem (purple, Sinha et al. [2011]), Dandak speleothem (Orange, Sinha et al. [2007]), and the present study (Blue). The shaded light blue and red blocks bracket periods of Little Ice Age and Medieval Warm Period respectively. The arrows point to the corresponding events in the Jhumar cave reconstructions. The shift in the timeseries is due to two different methods adopted to reconstruct age models.*

Modern observations link weaker monsoon on land to enhanced convection in the eastern equatorial Indian Ocean(EEIO) [*Krishnan et al.*, 2006]. *Sinha et al.* [2011] proposed the controlling factors of such Mega-drought events to be seasonal dynamics of the ITCZ in the EEIO. The southward migration of ITCZ in the Indian ocean prompts enhanced convection over the EEIO, which suppresses the convection and rainfall over India. Since the end of LIA, monsoon intensity has increased in 19th and 20th century, and entered an "active" phase of mon-

soon as described by *Sinha et al.* [2011]. The monsoon reconstruction based on Dandak-I stalagmite sample for 19th and 20th century is obscure and has low resolution owing to the errors in the age model. Recourse is taken to comprehensive tree ring studies to understand the climate change during this time period. *Shah et al.* [2007], based on tree ring width index of Hoshangabad observed several low rainfall years: AD 1835–1849, 1872–1896, 1908–1929, and 1952–1971. Comparison between $\delta^{18}O$ of annually resolved speleothem from Akalagavi cave and the Hoshangabad tree ring data shows that the monsoon rainfall increased from AD 1860 to 1940 reconstruction [*Shah et al.*, 2007]. Whereas tree ring studies from Parambikulam, Kerala [*Bhattacharyya et al.*, 2007] reveal there were several multi-decadal events of low and high precipitation in the last 1000 years. AD 1743–62, 1794–1806, 1815–26, 1831–51, 1856–76, 1937–56 were observed to be low rainfall events alternating with high rainfall events at AD 1763–93, 1807–14, 1827–30, 1852–55, 1877–1936, 1957–77 and 1995–98. However, most of these fluctuations were observed till the end of 19th century and the 20th century is inferred to be remarkably warm with higher rainfall [*Bhattacharyya et al.*, 2007].

4.6.4 Global teleconnections

Understanding the Holocene climate variability is of prime importance, and the teleconnection between high-latitude and low-latitude climate changes. If solar forcing is the main cause of climate change, then the tropics receiving large amount of radiation, are the hotspots for capturing the signal and communicating the amplified signal to higher latitudes through different mechanisms of heat transports [*Yin and Battisti*, 2001]. Superimposed on these long-term variations, are the millennial scale changes that can not be explained using only orbital parameters (e.g., *Gupta et al.* [2003]). Such millennial scale variations are partly attributed to abrupt changes in the North Atlantic, European and Eurasian climate, on the basis that increase in winter snowfall over Eurasia leads to a weaker monsoon over Asia the following summer [*Barnett et al.*, 1989; *Gupta et al.*, 2003;

The North Atlantic changes are mainly witnessed as large scale climatic events know as 'Daansgard-Oeschager' cycles during the last glacial period and 'Bond events' during the present interglacial period. The Bond events were reported in the cores raised from the North Atlantic Ocean and were observed to recur at an intervals of 1470 $\pm$ 500 years. These episodes, preserved as ice rafted debris are linked to sudden cooling of ocean surface water, brought about by changes in the North Atlantic surface circulation [*Bond et al.*, 1997]. These ice rafting deposits are related to change in the thermohaline circulation due to a southward shift of cooler ice-bearing surface water into the North Atlantic and its coupling with the Greenland atmospheric circulation changes [*Bond et al.*, 1997]. However, the constant pacing of these events is not controlled by ice sheet oscillation directly and the forcings governing the millennial scale changes are still to be identified. The coeval increase of the North Atlantic temperature with increase in monsoon precipitation between 10.4 -9 ka (Figure 4.16), along with the evidence of Bond events (10.3 and 9.4 ka) in the core monsoon region of India, confirms the strong link between the two. The evidence of such a relation is also reported in a speleothem from the Qunf cave [*Fleitmann et al.*, 2003] and Arabian Sea sediment cores [*Overpeck et al.*, 1996; *Schulz et al.*, 1998; *Sirocko et al.*, 1993]. *Fleitmann et al.* [2007], relate the 9.4 ka event to the outburst of melt water, resulting in the weakening of thermohaline circulation and the subsequent cooler North Atlantic temperatures. Such temperature changes are also observed in Greenland ice core records NGRIP, GRIP [*Johnsen et al.*, 2001]. The Greenland temperature oscillations reconstructed from ice cores, have a direct impact on the climate variability in Northern and Central Europe, with concomitant changes in ISM. The important feature of GISP-2 and GRIP $\delta^{18}O$ records is relatively smaller fluctuations during Holocene, implying no significant changes in temperaure during the past 10 ka BP. However, a 300 yr running mean of bidecadal $\delta^{18}O$ values show low frequency climate changes [*Schulz and Paul*,

2002],

The winter cooling and concomitant increase in the Eurasian snow cover led to weakened monsoon circulation through the well-known snow cover- monsoon linkage (e.g., [*Barnett et al.*, 1988; *Ye and Bao*, 2001]). Due to the extensive snow cover over western Eurasia, spring heating of the landmass is reduced on account of high albedo and high energy consumed in exhumation of excess snow. The reduction in land - sea pressure gradient due to the cooling of the Tibetan plateau in summer leads to weaker summer monsoon. The reduced pressure gradient also affects the strength of cross-equatorial current, which is the predominant source of moisture and heat.

ISM not only responds to the North Atlantic changes during the glacial period, but also has a huge impact on centennial and millennial timescales. Abrupt Holocene cold spells of North Atlantic correspond to a weaker monsoon over India (Figure 4.18 [*Bond et al.*, 1997]). Bond events, in mid- and late Holocene (0 to 4) are more prominent than the events 5 - 7 (Figure 4.15). Widespread aridity is observed between 6 - 5.2 and 5 - 3.9 ka BP. The major event 3, which marked the decline of major civilizations such as the Harappan, the Neolithic culture of central China and the Akkadian empire in Mesopotamia $\sim 5-3.5$ ka BP is related to strong aridity over India [*Giosan et al.*, 2012; *Kenoyer*, 1998; *Possehl*, 2002], western china [*Wenxiang and Tungsheng*, 2004] and western Asia, respectively [*DeMenocal*, 2001]. This implies that subtle changes in North Atlantic Climate may have significant impact on ISM.

To sum up, some hypotheses proposed by previous workers about continuous increase or decrease of monsoon throughout the Holocene have failed to explain the observed variability in the present study. According to our observations, the monsoon over India increased rapidly with rising insolation followed by a gradual decrease in monsoon between 8-6 ka BP. However, post 6 ka BP, an abrupt decline in monsoon is observed possibly as the feedback mechanisms accentuated the forcing factors leading to the failure of response of the monsoon system.

Between 3.5 - 2.5 ka BP prominent increase in monsoon, comparable to present, is observed. In spite of insolation being minimum at present, strengthening of monsoon is seen from 2 ka to the present, suggesting, on a millennial timescale, the ISM intensity is controlled by other factors, along with insolation.